Analysis of Solar PV Glare in the Urban Environment

Ishangiri Goswami

Delft University of Technology

TU Delft

Analysis of Solar PV Glare in the Urban Environment

by

Ishangiri Goswami

to obtain the degree of Master of Science
at the Delft University of Technology,
to be defended publicly on Monday November 30, 2022 at 02:00 PM.

Student number:	5359937	
Project duration:	February 1, 2022 – November 30, 2022	
Thesis committee:	Prof. dr. ir. I. Gordon,	Part-time Professor, PVMD/ESE
	Dr. H. Ziar,	Assitant Professor, PVMD/ESE (Supervisor)
	Dr. M. Cvetkovic,	Assitant Professor, IEPG/ESE
	Ir. Y. Zhou,	TU Delft, Daily Supervisor

TU Delft

Preface

This report is written as a Master thesis under the program Sustainable Energy Technology under Electrical Engineering, Mathematics, and Computer Science. The Master thesis project will be defended in front of a committee involving Prof. Dr. Ivan Gordon (PVMD/ESE), Dr. Hesan Ziar (PVMD/ESE, supervisor), and Dr. Milos Cvetkovic (IEPG/ESE: External Committee Member). The project work is done under Ir. Yilong Zhou as daily supervisor and Dr. Hesan Ziar as the project supervisor.

The main objective of the project was to develop a new tool that can predict the glare from the reflected light from PV systems in urban environments. The theories involved in developing the tool are explained in detail in this report. The analysis using the developed tool was carried out at various locations around the Schiphol airport to check if the glare created from the reflection from the PV system affects the flight path.

Resources and research by professors, researchers, and peers were used extensively in this project. The results obtained under this project will be a part of the collective research knowledge base of the Photo-voltaic Materials Department (PVMD) group.

Ishangiri Goswami
Delft, 30 November 2022

Acknowledgement

I would like to thank project supervisor Dr. Hesan Ziar. This project would not have been possible without his continued support. The knowledge and help received from the Hesan was immensely helpful in concluding the project. I would also like to thank Ir. Yilong Zhou. His explanation of the objective of this project motivated me to join this project. Yilong was always available for helping me with discussion of various theories and developing a model by coding. Hesan and Yilong created a supportive environment for me to work on this project. I would especially like to thank Prof. Dr. Ivan Gordon and Dr. Milos Cvetkovic for taking time out of their busy schedule to attend my defence thesis and agreeing to become the committee member in the defence.

I would also like to thank the researchers and my peers in the PVMD group who helped me with my project with their valued feedback. I would also like to thank my friends for their continued support. Lastly, this would not have been possible without my family's support. I am always grateful to my family for their continued support.

Summary

There is a mass migration of people towards urban areas. In a few years, most of the world's population will live in urban conglomerates. This can result in high congestion in energy grids. Governments are providing subsidies to people installing rooftop PV. Also, rooftop PV can be very advantageous, especially in energy costs for people in urban areas. Hence, the amount of rooftop PV is increasing. Additionally, PV in airport areas is becoming more popular with the advent of CO2-neutral airports. These PV systems are designed to absorb a high amount of light. There is still some reflection from these panels. This reflection can be the source of glare in these environments. In urban environments, it can be a nuisance. In areas near airports, roads, and railway lines, glare can result in accidents.

The main objective of this project is to develop a tool to predict glare from reflection from PV panels. This was developed by combining theories of Schlick Single BRDF and Hazard plot proposed by Clifford K. Ho. The Single BRDF predicts the direction and amount of reflection from a reflecting surface. Hazard plot predicts whether reflected light results in glare. The results of reflection with high and low potential for after-image creation are presented in the spherical and fish-eye view.

The glare prediction from the tool should be conducted for new PV systems in urban environments to determine the optical safety of the system. A case study for the same objective is conducted at a few locations near Schiphol airport. Four different locations are selected for conducting analysis. Installation of PV systems at the first location is not suitable due to the issue of reflection on the flight path. The PV system in the second location is the most suitable as there is no interference of glare and reflection on the flight path. Finally, PV systems at the third and fourth location can be very dangerous as the glare from these PV interfers with the flight

Contents

List of Figures

List of Tables

1 Introduction

The share of renewable energy sources has been increasing in the past few decades. One of the popular sources is Photovoltaics(PV). In today's world, about 4.4 billion people live in urban congregations. This number is expected to double by the year 2050[1]. In these urban settings, rooftop PV is very advantageous. Rooftop PV cuts back on energy costs. Additionally, it de-densifies the grid. Hence, subsidies are available from governments for the installation of rooftop PV. Currently, 25 million houses completely or partially rely on rooftop PV systems for their energy. This number is expected to reach 100 million by the year 2030[2]. Increasing rooftop installations in low-rise buildings in the urban environment would result in glare and reflection in high rises. The share of energy production by PV would be increasing in the future and many of these systems would be near and around airports with the advent of Carbon neutral airports[3]. Hence, PV installations near empty areas of airports are becoming increasingly famous.

Figure 1.1: PV system on Private House in Hangelar, Germany [4]

Figure 1.1 shows discomfort caused by rooftop PV systems in the urban environment. In the urban environment, the highest impact can be discomfort from reflection or the creation of after image due to reflection. But in the airport environment, on roads, or near railway lines, this reflection or glare can result in an accident. There have already been 58 accidents reported due to high light intensity till 2004[5]. These accidents mainly occurred during landing or take-off. Not only do these PV systems affect flights, but they also affect Air Traffic Control towers (ATC). In 2012, Manchester-Boston regional airport had to cover the PV system installed near it due to blinding reflection every morning at ATC towers[6]. The PV system had to be rearranged so as to not have that issue. Hence, there is a need to analyze how these systems would create reflections and glare in the urban neighborhood. Figure 1.2 shows how the PV installations near the airport can be dangerous due to reflection from the system.

Figure 1.2: PV System at Tucson International Airport, USA [7]

Primary objective of this project is to develop a tool that can predict the glare and reflection occurring from the PV system. The steps involved in developing the tool are described below:

1. The function theorizing reflection from reflecting surface
2. Finding specific threshold where reflected light creates glare
3. Considering the urban construction and skyline
4. Considering light obstruction and shadow of the urban construction
5. Validate the newly developed model.

In this report, in chapter 2, the details about approaches and metrics already present in the market are discussed. In chapter 3, theories involved in developing the new model will be discussed. A deep dive into the Bidirectional Reflectance Distribution Function (BRDF) and the potential for glare from reflection will be done. In chapter 4, a discussion on details about the input of data for the developed model and functions required for the smooth running of the model is carried out. Additionally, in chapter 5, the methodology to develop the model is explained. The model is validated which is shown in chapter 6. In chapter 7, the obtained results are explained in detail. The observations based on these results are made. Finally, important conclusions are derived in chapter 8 from the obtained results.

2
Market Research

PV systems are designed to absorb a high amount of light. There is still a reflection of about 7.15% reflection from the PV which are specifically designed for airports[8]. The approaches and metrics available in the market to analyze reflection have been divided into three different types. These three types of approaches are Site Visit based, Hybrid, and Computer based approaches[9]. The more prevalent approaches are shown in table 2.1.

<table>
<tr><th rowspan="2">Site Visit Based</th><th rowspan="2">Hybrid</th><th colspan="2">Computer Based</th></tr>
<tr><th>Non-Commercial</th><th>Commercial</th></tr>
<tr><td rowspan="4">Helicopter Flyover/Drive-by Approach</td><td rowspan="2">Image Synthesis Based</td><td>CFD</td><td>Solar Glare Hazard Analysis Tool (SGHAT)</td></tr>
<tr><td>Ho et al. Approach</td><td>FORGESOLAR</td></tr>
<tr><td rowspan="2">Reflection Protractor</td><td rowspan="2">Wollert and Rose Approach</td><td>Zehndorfer’s Tool</td></tr>
<tr><td>Fraunhofer ISE Tool</td></tr>
</table>

Table 2.1: Types of Glare Assessment Approaches[9]

2.1. Site Visit Based Approaches

2.1.1. Helicopter Flyover/Drive-By Approach

In this approach, the helicopter is boarded and flown over the PV source. Digital photographs of the reflecting source are taken and further analyzed. The passenger would look at the reflecting source from the Helicopter and would notice if it creates glare or after-image. Similarly, a drive-by can be performed to check if the reflecting source or PV system near a road can be a reason for glare or the creation of glare or after-image.

This approach was used by Clifford K. Ho[10] to assess the glare from the system and whether the approach of plotting hazard developed at Sandia National Laboratory (SNL) is valid or not. The Helicopter Flyover was performed near the SNL facility in Albuquerque, New Mexico at the Concentrating Solar Power (CSP) plant. It was found that the reflection was enough to cause a glare that happened at a distance of more than a mile (1700 m) at a height of about 580 m. Figure 2.1 shows the test conducted by Helicopter Flyover.

Also, the drive-by was also performed by them at Highway 95 near Boulder city, Nevada, and the result is shown in Figure 2.2.

This approach is highly sensitive to the time of the year as well as the location. The site visit based approach cannot be scaled up to other locations, nor can it be scaled up to give results throughout the year without having the data from the site for the given time period.

2.2. Hybrid Approaches

2.2.1. Image Synthesis Based Approach

In this method, the luminance of office-like space is studied. This luminance data is gathered from digital High Dynamic Range (HDR) Photography. The threshold luminance from image synthesis in office-like space is studied by Wymelenberg et al.[11].

Figure 2.1: Helicopter Flyover near CSP at Albuquerque, NM[10]

Figure 2.2: Road Drive-by on Highway 95 in Boulder city, NV[10]

There are two metrics to assess the luminance threshold for glare assessment. One of the metrics is the Daylight Glare Probability metric (DGP)[12]. DGP can be given by Equation 2.1 as shown below.

$$DGP = 5.87 * 10^{-5} * EV + 9.18 * 10^{-2} log(1 + \sum \frac{Ls^2 * \omega^2}{EV^{1.87} * P^2}) \quad (2.1)$$

The DGP value above 0.45 can be understood as having disturbing daylight glare. Here EV is the vertical illuminance at eye level [lux], Ls is the luminance of the source [cd/m2], ω is the solid angle of the source [sr], and P is the Guth position index. The luminance data is gathered from RADIANCE[13]. A new tool named Evalglare is developed for getting the Daylight Glare Probability[12].

The second metric for finding the luminance threshold is Daylight Glare Index[14]. Similar to DGP, the luminance data required can be obtained from RADIANCE. The DGI can be calculated from Equation 2.2 as shown below.

$$DGI = 10 * log(0.478 * \sum \frac{Ls^{1.6} * \omega^{0.8}}{Lb + (0.07 * \omega^{0.5} * Lw)}) \quad (2.2)$$

The DGI values above 35 can be interpreted as serious daylight glare. This approach uses high computational memory because of the usage of RADIANCE and can mostly be used for office-like spaces or at the building level. It cannot be scaled up beyond that point.

2.2.2. Reflection Protractor

In this approach, simple tools are used in conjunction with laws of reflection. The intensity of the reflected light can be calculated using Hollayday formula[15]. The value of the intensity is then compared to the adapted value for the glare impact on the level of the human eye. This approach is quite laborious, as the method has to be repeated for every point in the environment.

2.3. Computer Based Approaches

There are many Computer Based approaches that can be generally divided into two parts. One of them is Non-commercial and the other is Commercial approaches.

2.3.1. Non-Commercial Approaches

Computational Fluid Dynamics (CFD)

In CFD analysis, temperature studies can be carried out using solar radiation and the reflective properties of materials. Softwares like ANSYS, COMSOL, etc. can be used for this analysis. In this approach, there are no considerations of material properties, panel azimuth, and tilt and solar incidence angles. Hence, only simple geometries are analyzed in CFD. Additionally, this approach takes up high computational memory even with simple geometries, as even analysis of one flat surface can take up Megabytes of space and minutes of run-time.

Ho et al. Approach

In Ho et al. approach, a look-back approach is adopted. The irradiance entering the eyes (retinal irradiance) is analyzed[16]. The retinal irradiance and the subtended source angle are used to plot the values on the hazard plot as shown in Figure 2.3. The points lying on 'green' have a low potential for after-image. The points lying on 'yellow' have a high potential for after-image. Lastly, the points lying on 'red' have the potential for permanent eye damage.

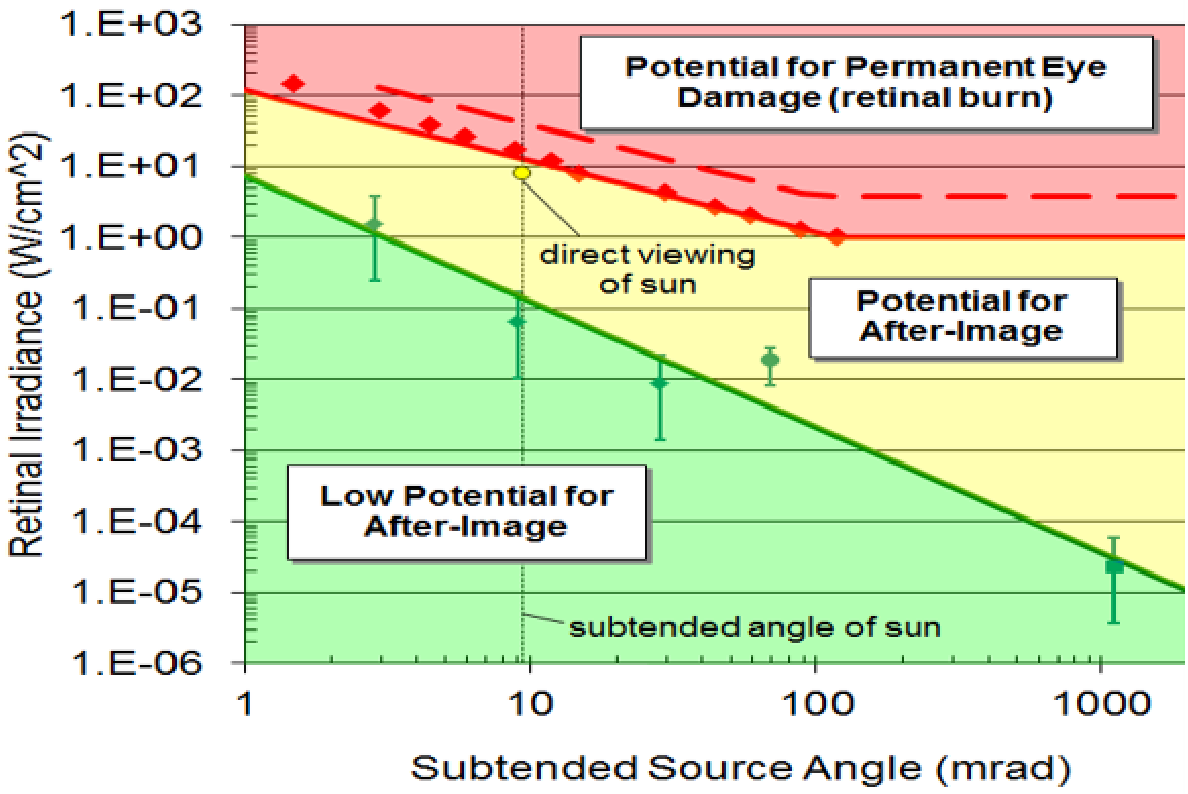

Figure 2.3: Potential Impacts of Retinal Irradiance as a function of Subtended Source Angle for 0.15s exposure (Hazard Plot) [16]

Ho et al. approach is used in Solar Glare Hazard Analysis Tool (SGHAT) and FORGESOLAR. More details about Ho et al. approach will be explained in chapter 3 in section 3.2.

Wollert and Rose Approach

To assess the effect of reflection from PV modules, Alexander Wollert and Thomas Rose [4] consider the Reflectance function. Specifically, the Schlick Reflectance model or BRDF model is used. There are many Reflectance models available, either empirical or theoretical. But the Reflectance function from Cristophe Schlick, also known as the BRDF model was chosen in this approach[17]. The BRDF function would be explained in detail in Chapter 3 in section 3.1. Schlick model is an intermediary approach. This means that this model has physical validation and is not very computationally heavy. This would be explained in detail in chapter 3 in section 3.1. BRDF is given as the ratio of irradiance reflected and irradiance incident on the reflecting surface shown in Equation 2.3.

$$BRDF = \frac{ReflectedIrradiance}{IncidentIrradiance} \tag{2.3}$$

The Wollert and Rose approach considers the day and time of the year to assess the reflection from the PV module. A computer tool has been developed based on this approach at Fraunhofer ISE which shows the tabulated results. This tool will be explained later in this section. In this approach, only reflection from the PV module is considered and no quantification of the glare is given.

2.3.2. Commercial Approaches

Solar Glare Hazard Analysis Tool (SGHAT)

SGHAT is a tool developed at SNL using Ho et al. approach. This tool is Federal Aviation Administration (FAA) approved. Currently, SGHAT tool usage is restricted, although freely available to public departments in the US and SNL internal usage.

The location of the site of interest can be selected from interactive maps from Google. Also, PV system designs such as PV tilt and azimuth can be manually selected. Similarly, PV material can be selected from the list of available materials in the tool. This list includes materials like smooth glass with/without anti-reflection coating, light textured glass with/without anti-reflection coating, and deeply textured glass. The tool assesses the time of the year when the potential of after-image occurs, which can be shown in Figure 2.4. These results are derived from the Hazard plot shown in Figure 2.3. Furthermore, different angles of azimuth and tilt are assessed to check the reduction in glare without much reduction in power output.

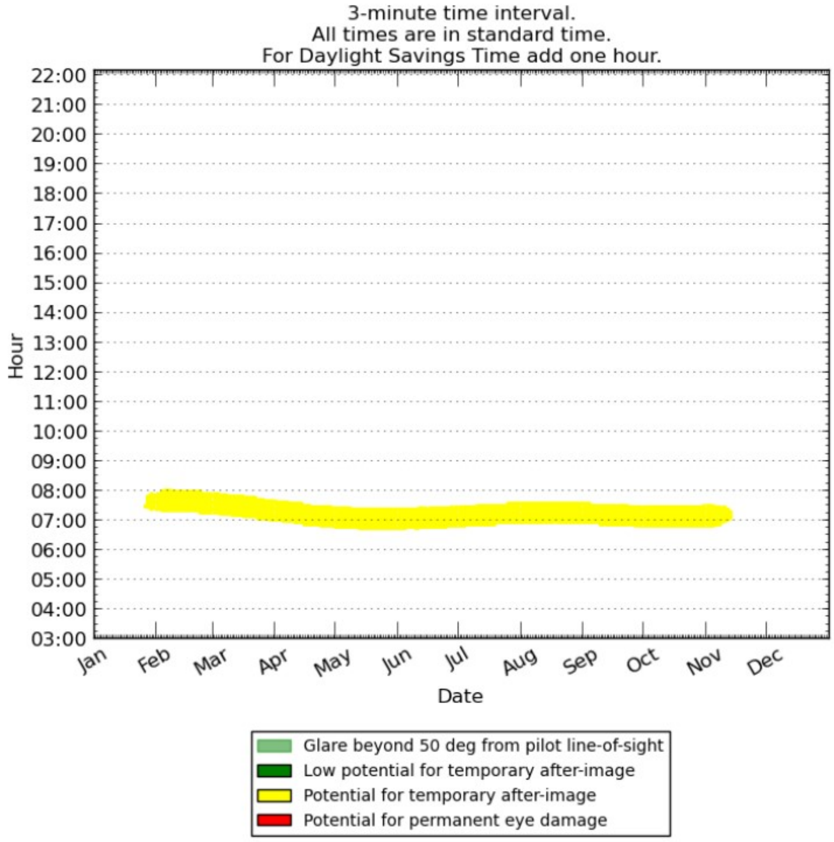

Figure 2.4: Potential Impacts of Retinal Irradiance as a function of Subtended Source Angle for 0.15s exposure (Hazard Plot) [18]

ForgeSolar

ForgeSolar is a tool based on SGHAT from SNL. This was licensed to Sims Industries in the year 2016. Sims industries have been improving on SGHAT for the past few years. The pricing of the software ranges from $40 to $270 monthly depending on the usage and tools included.

In ForgeSolar, the tool named GlareGauge provides results similar to the one shown in Figure 2.4 for any chosen location in the world. Additionally, GlaReduce provides the best configuration for panel tilt and azimuth for a given location. Similar to SGHAT, it does not consider the topography of the location or urban environment.

Fraunhofer ISE tool

Engineers at Fraunhofer ISE developed a solar reflection tool that delivers results similar to those in Wollert and Rose approach. This tool takes the urban environment and topography of the location into account including the effects of obstruction and shadowing. The tool gives the reflection result throughout the year. Also, the user can choose the PV tilt, azimuth, and the material of the module.

The glare hazard is assessed based on the time duration of reflection. There is no consideration of Ocular safety in this tool. Ocular safety is the assessment and removal of hazards that may cause injury to the eye.Ocular safety is safety concerning the human eye from light perception. This software is used by engineers at Fraunhofer ISE for reflection assessment requested by clients.

Zehndorfer Glare Assessment Tool

Software is developed by Zehndorfer Engineering for glare assessment from reflecting surfaces like building facades, PV panels, etc. The tool considers obstruction and shadowing occurring in the urban environment and building footprints.
Some of the results obtained from this tool are as follows:

- Topography of location
- Glare-Time diagram in a horizon for a given day
- Frequency of glare
- Impact of glare

The tool uses backward ray tracing for determining the direction of reflection, which can be computationally slower. For the impact of glare, a tool at Zehndorfer Engineering uses the hazard plot as shown earlier. This tool is used internally to assess the glare of reflecting surfaces in urban environments requested by clients.

2.4. Need for New Glare Assessment Tool

There are different kinds of assessment approaches already available in the market. The site visit based approaches are only useful for a definite location at a defined time. These approaches cannot be used to get results throughout the year or at any location without experimental data after visit. Similarly, Hybrid approaches rely on data taken from the location of interest. These approaches are either computationally heavy, numerically tedious, or restricted to smaller spaces.

To achieve glare results throughout the year for different locations, the better approaches are the ones that are Computer based. Many commercial and non-commercial approaches are available. Out of these approaches, only the Zehndorfer Glare Assessment tool gives results for glare impact and direction of reflection with the inclusion of the urban skyline. Other tools do give either result, but not both. But as this tool uses backward ray tracing, the simulation can be very computationally heavy. Therefore, there is a need in the market for a tool that assesses the reflection including the effects of shadow/obstruction and impact of glare as a function of ocular safety which is not computationally heavy.

The new tool which is to be developed should consider ocular safety and should show the direction of reflection without being very computationally heavy. Hence, the new tool will be based on the Reflectance model, which predicts reflection direction and intensity, especially the Schlick Reflectance model (BRDF) which is accurate and not very computationally expensive. Besides, glare impact would be assessed from the Hazard plot proposed in Ho et al. approach. The theory behind these two factors would be studied in further detail in chapter 3.

3

Background

In order to predict the direction and the effect of reflection on ocular safety or saf, the newly developed model shall meet the following three requirements:

- Find the irradiance of light reflected from the reflecting surface, or in our case, PV panels
- Determine the direction of reflection from the reflecting surface
- Determine the effect of irradiance of reflected light on ocular safety and whether this light would create glare

3.1. Bidirectional Reflectance Distribution Function

There are many models available to speculate the irradiance of specular reflected light. These models can be generally divided into three types. The first type of models are theoretical, which still lacks validation. The second type of models are empirical models. These models are unnecessarily accurate, and hence computationally heavy. The third type of models are an intermediary between theoretical and empirical models, which are computationally inexpensive and have validity in the real world as well. These models are shown below in table 3.1.

Theoretical Models	**Empirical Models**	**Intermediary Models**
Torrence-Sparrow Model	Phong Model	Schlick Model
Cook-Torrence Model	Blinn-Phong Model	Ward Model
He-Torrence-Sillion-Greenberg Model	Lafortune Model	
	Lebedev Model	

Table 3.1: Types of BRDF Models [19]

The first intermediary model was given by G.J. Ward[20]. This model is an approximate model and does not follow the Fresnel effect[19]. Another intermediary model which follows the Fresnel effect is the model proposed by Cristophe Schlick[17]. This model is computationally light, and has physical validity. Hence, Schlick model was selected to analyze the irradiance and direction of reflection.

3.1.1. Schlick BRDF Model

Schlick proposed the intermediary BRDF model which follows the Energy Conservation law, Helmholtz reciprocity theorem, Microfacet theory, and Fresnel effect. Additionally, the model considers the isotropic and anisotropic properties of the material.

The model for homogenous material is called Single BRDF. Meanwhile, the model for heterogeneous material is called Double BRDF. The reflection from one layer of homogenous materials like glass can be analyzed through Single BRDF. The reflection from plastic materials, or materials, where reflection from two materials plays a role can be analyzed through Double BRDF. The reflection from the panel is considered as the reflection from the first layer of glass as other layers are designed to absorb maximum incoming light. Hence, Single BRDF from the Schlick model is used.

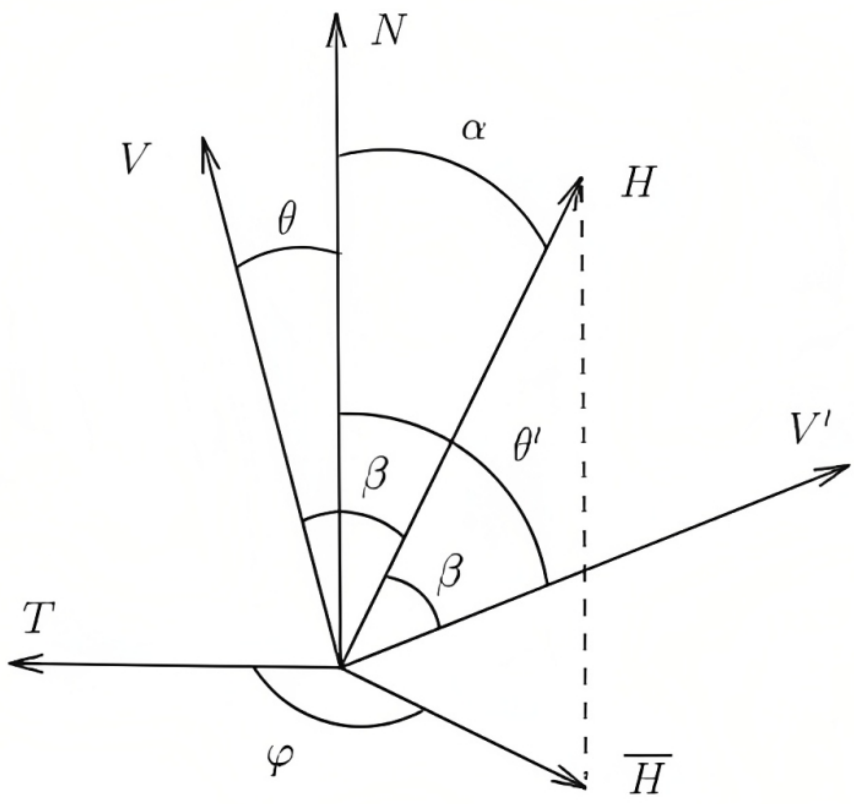

Figure 3.1: Angles and Vectors involved in Schlick BRDF Model [17]

The figure 3.1 shows the geometry involved in the BRDF model. The vector representation shown in thee figure above is represented in 2-D plane of direction north-south and vertical direction. The origin in the figure is the reflecting surface, in our case the PV panel. The vectors involved in the geometry are as follows:

- N: Surface Normal Vector
- T: Surface Tangent Vector
- V: Outcoming Direction
- V': Incoming Direction
- H: Facet Normal Vector
- $\overline{H}$: Projection H - N

Similarly, the angles involved in the geometry are as follows:

- α: Panel tilt (<H,N>)
- ϕ: Panel azimuth
- β: Angle of reflection and Angle of incidence (<V,H> = <V',H>)
- θ': Solar Zenith angle (<V',N>)
- θ: Angle of reflected light with respect to direction up <V,N>

Now the cosine of all the angles which are used in this theory is shown below:

- cos(α) = t

- cos(β) = u
- cos(θ) = v
- cos(θ') = v'
- cos(ϕ) = w

After understanding the vectors and angles involved in BRDF geometry, we will dive deeper into finding the value of BRDF (R_λ). Single BRDF can be expressed as a function of spectral influence (S_λ) and directionality (D). This is expressed in Equation 3.1.

$$R_\lambda(t,u,v,v',w) = S_\lambda(u) * D(t,u,v,v') \tag{3.1}$$

The spectral influence in Single BRDF is the function of the Reflection Factor at wavelength λ. The Reflection Factor is value of Reflectance at normal incidence. The spectral influence is dependent on incident angle of light. This can be shown in the Equation below.

$$S_\lambda(u) = C_\lambda + (1 - C_\lambda) * (1 - u)^5 \tag{3.2}$$

In the simplest form, spectral influence can be equated to the Reflection Factor (C_λ ϵ [0,1]), but in this case, it does not follow Fresnel law. To overcome this issue, spectral influence has to be the function of incidence and reflection angle. Another factor involved in analyzing Single BRDF is the Directionality factor. The directionality factor can be shown in the Equation as below.

$$D(t,v,v',w) = \frac{1 - G(v)G(v')}{\pi} * A(w) + \frac{G(v)G(v')}{4\pi v v'} * Z(t) * A(w) \tag{3.3}$$

The Directionality factor has zenith angle dependence (Z(t)) and azimuth angle dependence (A(w)) as shown in Equation 3.4 and 3.5. These are ultimately dependent on the roughness (r ϵ [0,1]) and isotropy factor (p ϵ [0,1]) of the material.

$$Z(t) = \frac{r}{(1 + rt^2 - t^2)^2} \tag{3.4}$$

$$A(w) = \sqrt{\frac{p}{p^2 - p^2 w^2 + w^2}} \tag{3.5}$$

Equation 3.4 and 3.5 shows the zenith angle dependence and azimuth angle dependence as a function of the roughness factor and isotropy factor, respectively. In equation 3.3, the term G(v)G(v') represents self-shadowing with reemission. Schlick model predicts self-shadowing with reemission much more accurately without adding to the computational cost. This self-shadowing with reemission phenomenon can be mathematically formulated as shown in the Equation below.

$$G(v) = \frac{v}{r - rv + v} \tag{3.6a}$$

$$G(v') = \frac{v'}{r - rv' + v'} \tag{3.6b}$$

The peaks and troughs due to surface rouhgness of the material acts as obstruction to incident light. This obstructed light is reemitted which can be shown in Figure 3.2.

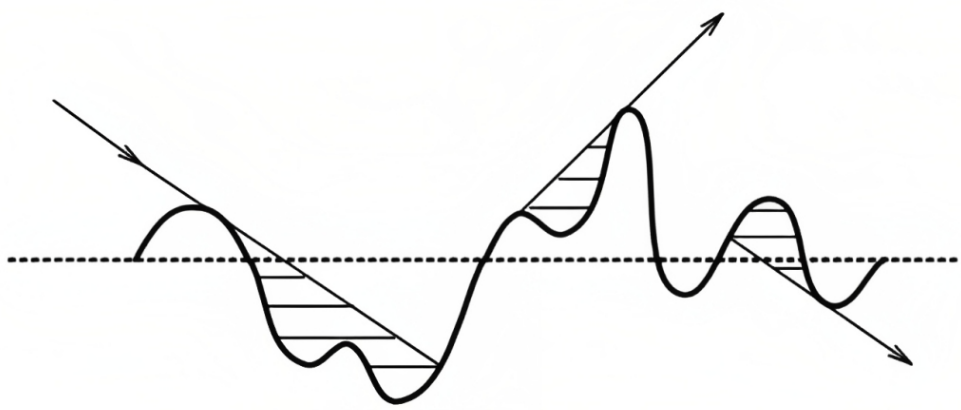

Figure 3.2: Self-shadowing with Reemission [17]

The Single BRDF can be used to find the irradiance of reflected light. Also, Single BRDF accurately determines the direction of reflection. Thus, first two requirements for developing the new model is met by this function.

3.2. Glare Hazard

In the study proposed by Clifford K. Ho[16], the study was done on the effect of intensity of reflection on a human eye. This is generally termed as Ocular safety. The empirical data is plotted as Retinal Irradiance (W/cm^2) vs Subtended Source angle (mrad) logarithmic graph. This graph is shown in Figure 2.3.

There are three regions in the graph. The green corresponds to retinal irradiance with a low potential for after-image. In other words, the glare in this region does not create danger. Secondly, the retinal irradiance falling in the yellow region has a higher potential of creating the after-image. These points create glare on the horizon and can be dangerous in urban environments. Lastly, the points in the red region create permanent eye damage and are extremely hazardous. It is worth noting that these empirical data are for 0.15s of light exposure to a human eye. This time scale is a realistic time exposure, especially for pilots having one point of reflection in their eyesight.
The equation of retinal irradiance can be given as shown below in Equation 3.7.

$$E_r = E_c \frac{(d_p)^2}{(d_r)^2} \tau \tag{3.7}$$

The retinal irradiance is function of corneal irradiance(E_c), pupil diameter(d_p), and the diameter created by the image at the retina(d_r).

In Figure 3.3, we see the anatomy of the eye and the terms involved in the calculation of E_r.

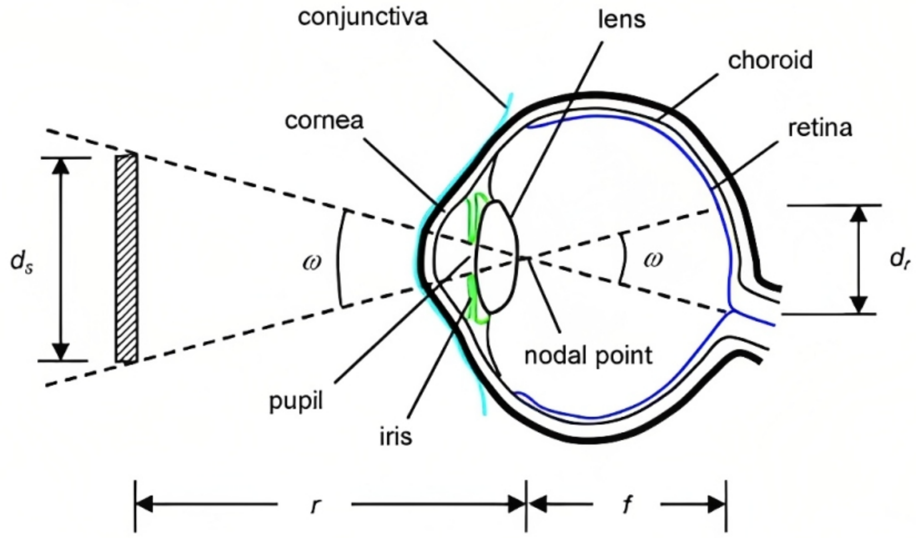

Figure 3.3: Anatomy of Image projected on retina [16]

The τ given in the above equation is called Transmission Coefficient. The value of τ is taken as 0.5 for a normal human eye. The pupil diameter for a normal human eye under the condition of perceiving light ranges between 2 mm to 4 mm[21]. In this case, d_p can be taken as 2 mm as the glare analysis is done under extreme light entering the eye. The image diameter on the retina is a product of the focal length and subtended source angle of the reflecting area. For the normal human eye, the focal length is 17 mm [22]. Subtended source angle is shown in Equation 3.8.

$$\omega = 2 * tan(\frac{d_s}{2 * r}) \tag{3.8}$$

Here, d_s is the source size and r is the distance between the observer and the reflecting area.

3.2.1. Collimated Beam

Now, the Single BRDF from Schlick model gives us the intensity of reflected light at the site of location. The collimated beam can be shown in Figure 3.4.

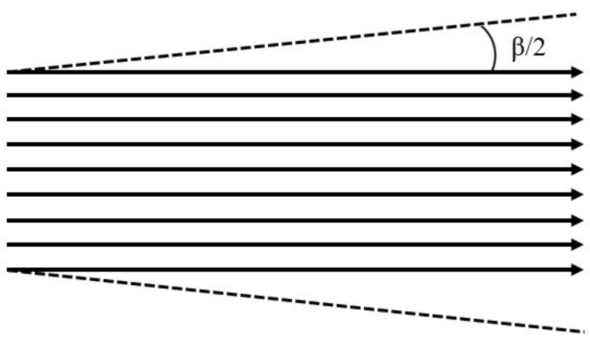

Figure 3.4: Collimated beam with sun half-angle deviation

Beam Divergence can be mathematically represented in Equation 3.9. As the angle is very small, the equation can be further simplified to Equation 3.10

$$BeamDivergence = 2 * r * tan(\frac{\beta}{2}) \tag{3.9}$$

$$BeamDivergence = 2 * r * \frac{\beta}{2} \tag{3.10}$$

This light travels a distance r to reach the observer's eye. This light beam travels as a collimated beam with a deviation of sun half-angle $\beta/2$. The value of the sun half-angle is about 4.7 mrad.

The analysis of glare is done at a distance of a maximum of 1 km, as the glare from PV panels is not hazardous beyond that distance[23]. Also, the intensity of reflected light from the Single BRDF is wavelength dependent. To conduct a study of glare from hazard plot, the irradiance entering the eye should be wavelength independent. To achieve this, reverse engineering is done to converge light to one beam from wavelength distributed light according to different atmospheric element transmissions[24]. This is done on the reflected light, hence we get the irradiance of reflected light which is wavelength independent. The main atmospheric elements which are considered for this are Water molecules, Oxygen, and Rayleigh Scattering.

4

Data Requirements and Acquisition

Before transforming these theories into MATLAB code, various functions involved and the data required beforehand will be discussed. Different channels of data gathering are discussed as well. This will be explained in detail in section 4.1. Furthermore, in section **??**, the pre-requisite MATLAB functions will be looked at in detail.

4.1. Input Data

To analyze the reflections from Single BRDF and predicting glare, a series of inputs are needed. These are listed as shown below:

- PV panel specifications
- Solar geometry (azimuth and altitude)
- Incoming solar irradiance
- Reflection factor
- Roughness and Isotropy factor
- Site details

PV panel specifications

Starting with, the geometry and structure of the PV panel can be obtained from the installed PV system. The inputs such as Panel tilt, Azimuth, and size are shown in Figure 4.1. The tilt angle of the PV panel can be interpreted as the complementary angle to angle α as shown in Figure 3.1. PV panel azimuth is the angle made by panel orientation respective to the direction North. This angle is denoted as ϕ shown in the explanation of Single BRDF. The length of the panel is denoted as l. There are some assumptions to keep in mind. First, the panel is considered a square. Also, if there is more than one panel in the system, it is considered as one big panel, and the gap between the panel is ignored. Lastly, if the panel size or system is big, the system has to be broken down into smaller systems to get accurate results.

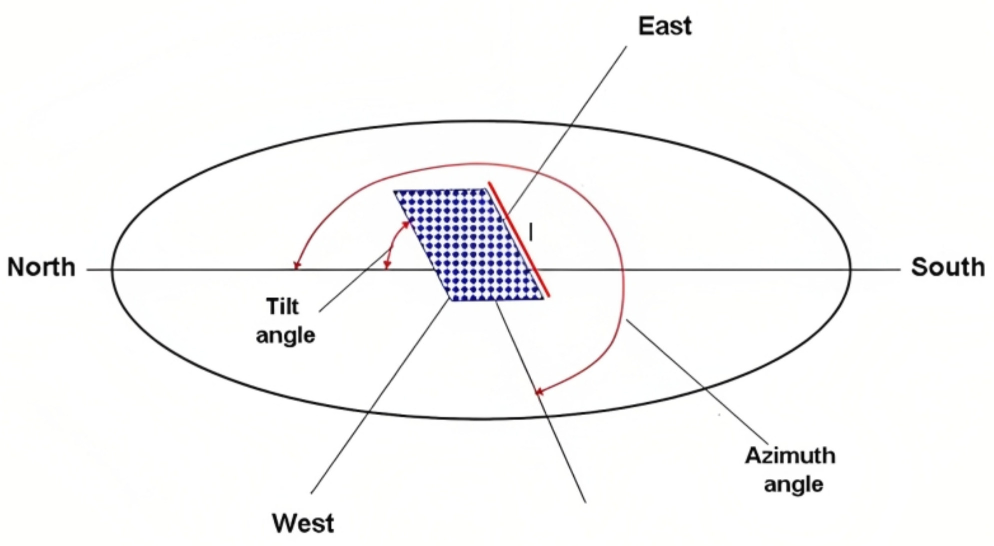

Figure 4.1: PV panel Geometry [25]

Solar geometry

The additional angles involved in the model are gotten from solar geometry. The first angle is solar azimuth, which is the angle of the sun's position relative to the North. Additionally, solar altitude is the sun's elevation and it is a complimentary angle to angle θ' (zenith angle) in Single BRDF. These two angles are then used to determine angles θ and β. These angles are shown in Figure 4.2.

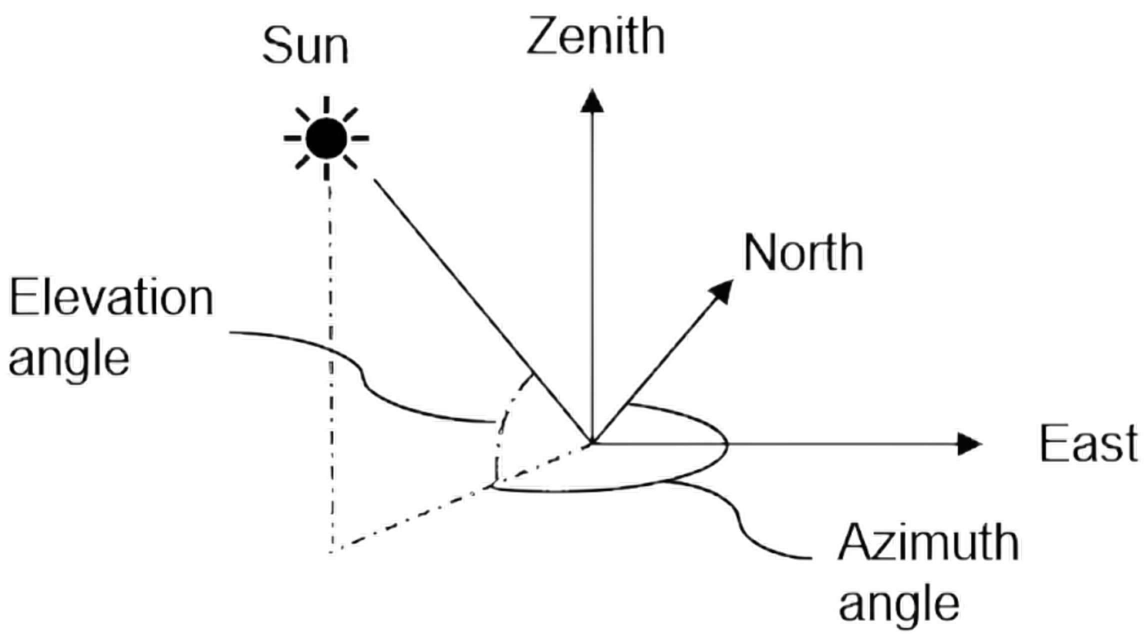

Figure 4.2: Solar Geometry

There are different methods of determining solar azimuth and altitude throughout the year. One of the methods is an experimental method like a solar tracking system which, for example, dual axis tracking system. This is also used to harvest maximum energy from incoming sunlight[26]. The trend shown from the data gathered this way is for the current time and not for the future. Another method for determining solar azimuth and altitude is through software like Meteonorm. Meteonorm gives the solar azimuth and altitude of the given location on an hourly basis. Additionally, the data gained from Meteonorm is experimental data. The trend seen is representative, but it can be used as an approximation for upcoming days.

Incoming solar irradiance

Another input needed for the model is solar irradiance. Incoming irradiation is called Global Horizontal Irradiance (GHI). GHI is the combination of Direct Normal Irradiance (DNI) and Diffused Horizontal Irradiance (DHI). This can be shown in Figure 4.3.

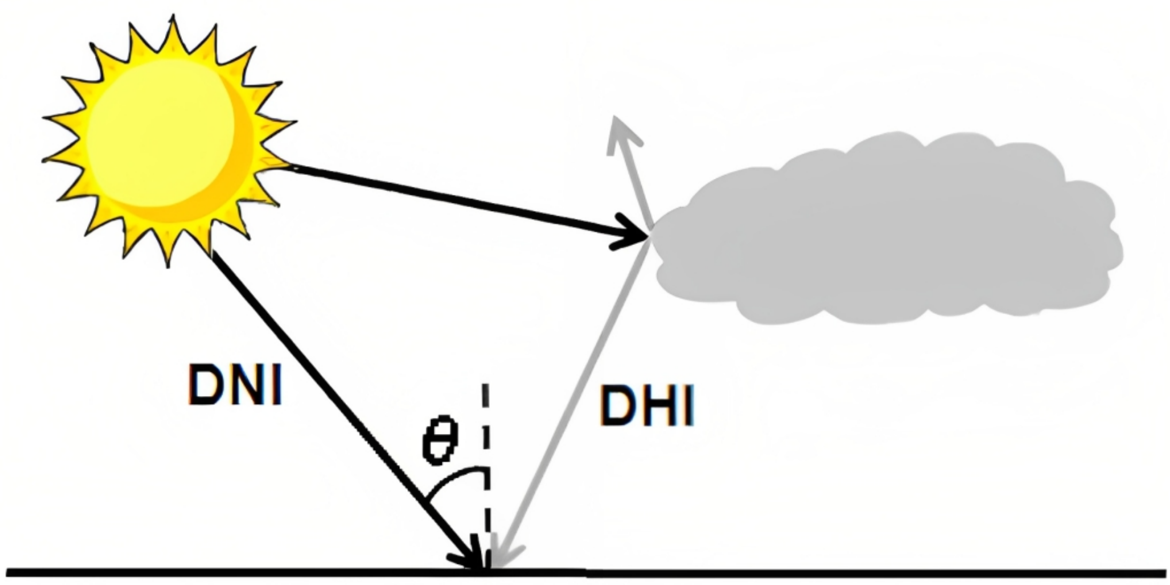

Figure 4.3: Solar Irradiance[27]

For PV, DNI and DHI is responsible for electricity generation. But only DNI is also responsible for reflection of visible light from PV. Thus, the input for the model is DNI and not GHI. Data for DNI can be gathered in two ways. The first way is to gather data experimentally. A 2-axis pyrheliometer is set up at the site of interest to gather data for DNI[28]. Pyranometers can be used to determine DNI as well, but they are less accurate than pyrheliometers. The second way of determining DNI is through software like Meteonorm. Similar to solar azimuth and altitude, DNI data from Meteonorm is on an hourly basis and historic.

Reflection Factor

The reflection factor is needed as input for the model. The Reflection factor is reflectance at normal incidence angle[17]. This can be gathered from instruments such as LAMBDA available at the Delft University of Technology. The mini-module has been made in-house to check the reflection factor. This mini-module is shown in Figure 4.4.

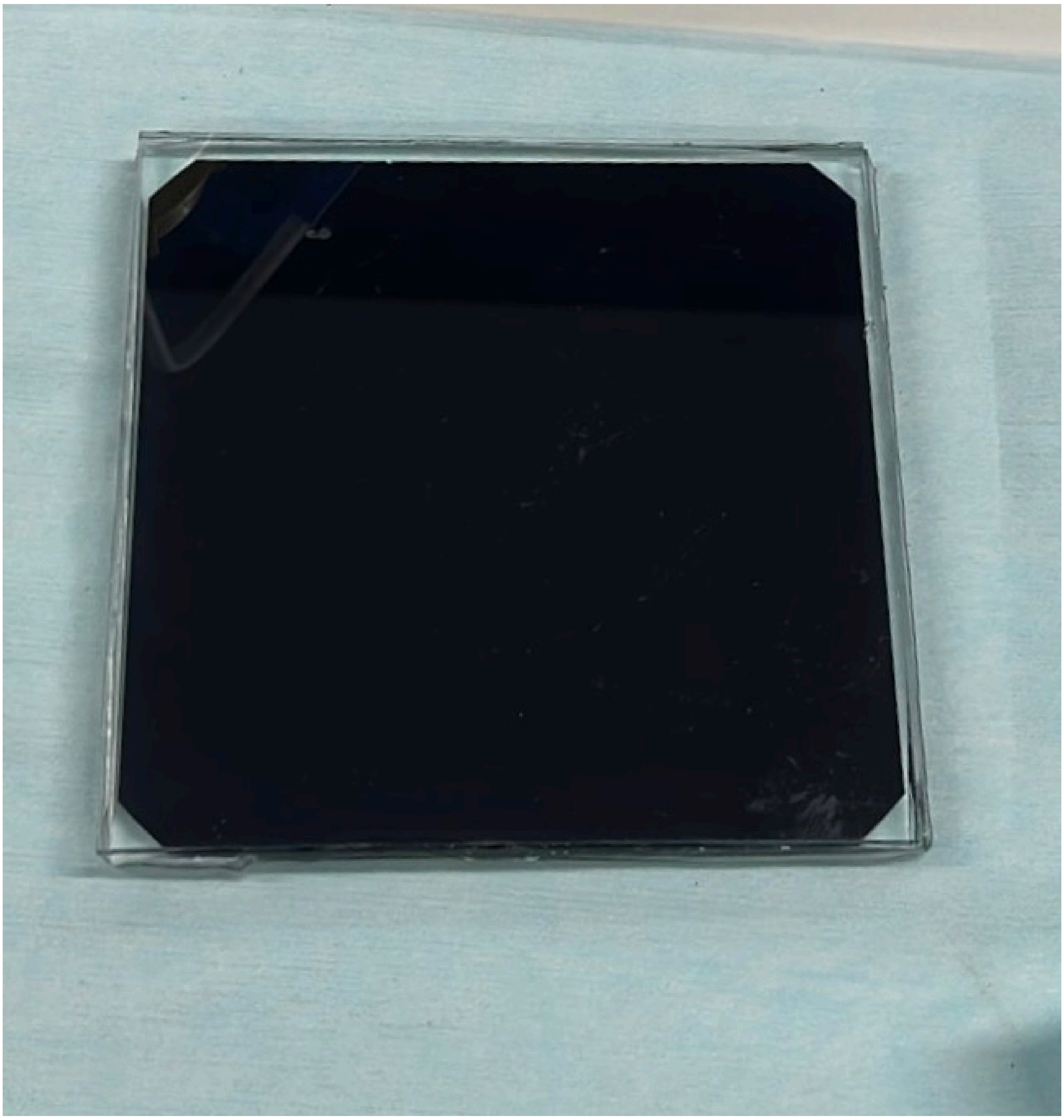

Figure 4.4: Reflection Factor of IBC module

This mini-module is set up in the designated testing area. The reflectance at normal angle is checked at every wavelength at defined gap. The laser with the given wavelength is projected on the testing material from a slit and the reflected light percentage is determined. The reflection factor is wavelength dependent. The data for the reflection factor for Integrated Back Contact (IBC) module is shown in Figure 4.5.

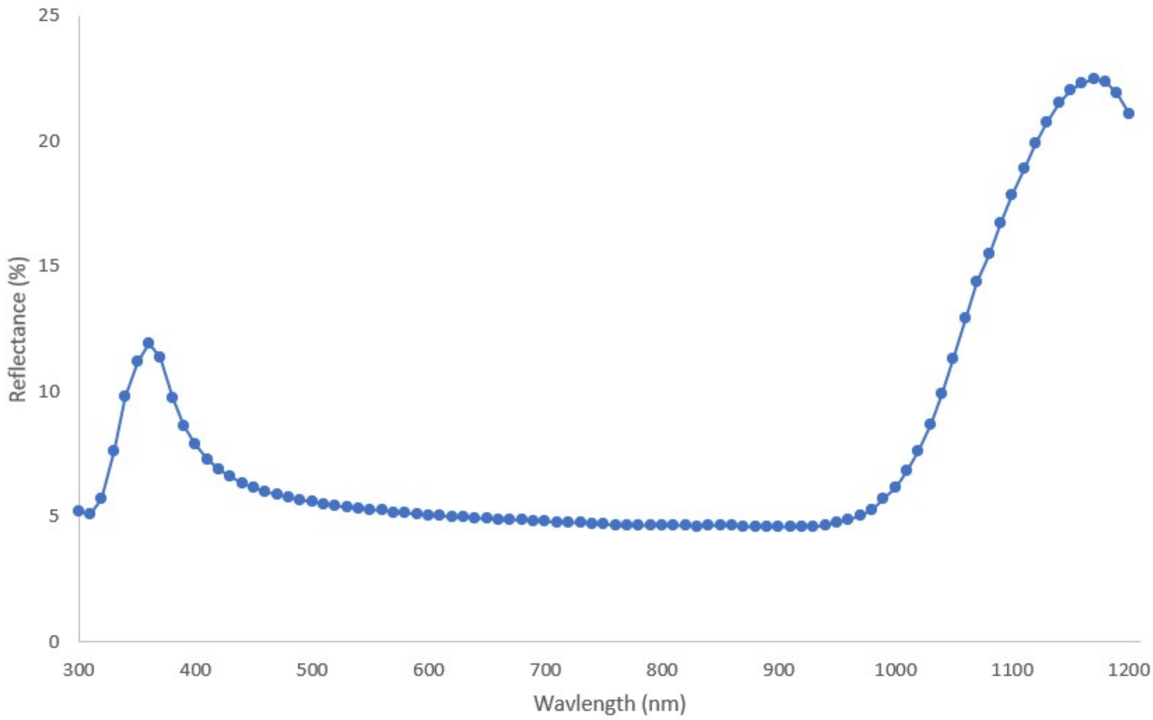

Figure 4.5: Reflection Factor of IBC module

Here, the data is shown for the wavelength range from 300 nm to 1200 nm. The PV panels working wavelength bandgap is 300 nm to 1200 nm. Hence, this bandgap is selected. The model is used for only one layer, i.e. the top layer of glass. The IBC module is selected to gather data as it does not have front metalization which ensures no reflection from the metal. The top layer is smooth glass.

Roughness and Isotropy factor

The roughness factor is used as an input for the model. The roughness factor is related to the RMS (Root Mean Square) slope of the surface. For smooth glass, the value of the roughness factor is 0.2[29]. This value can be determined experimentally as well. Instruments like Atomic Force Microscope can be used to determine the RMS slope of the material at scratch. The roughness factor can be given as RMS slope of roughness at scratch[30]. Additionally, the isotropy factor is needed as well. This can be determined as a factor of RMS slope at scratch (ϕ=0) and RMS slope at ortho-scratch (ϕ=pi/2). For smooth glass, this value can be taken as 0.8[31].

Site details

Final input needed is the details involving the site of interest. The first input is the coordinates of the site. The LiDAR data of the site is needed as well. Light Detection and Ranging (LiDAR) is carried through airplanes or helicopters. The light is sent as pulses to the ground and the time to receive the light at a sensor is recorded. This process is shown in Figure 4.6.

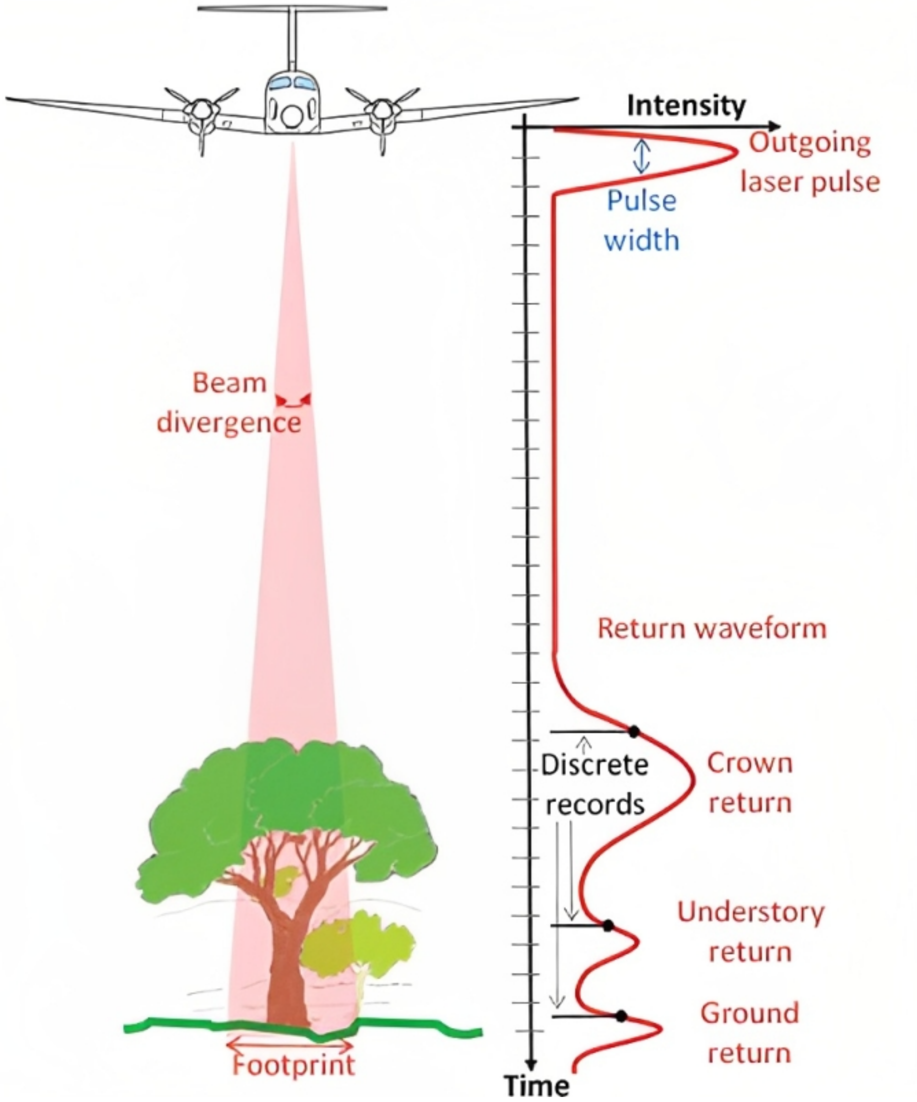

Figure 4.6: Airborne LiDAR data collection[32]

The light is returned from different points of the structure until it hits the bare ground. These are called the number of returns. The shapes of objects at these returns have different waveforms which project the shape of the object which is shown in the figure above. The point cloud of the height map is created with LiDAR data. This is obtained through Digital Elevation Model (DEM). The Digital Surface Model (DSM) shows the canopy of trees, roofs, construction, etc. Meanwhile Digital Terrain Model (DTM) specifically represents the ground surface. The point cloud of height is shown for a location in The Green Village in Figure 4.7.

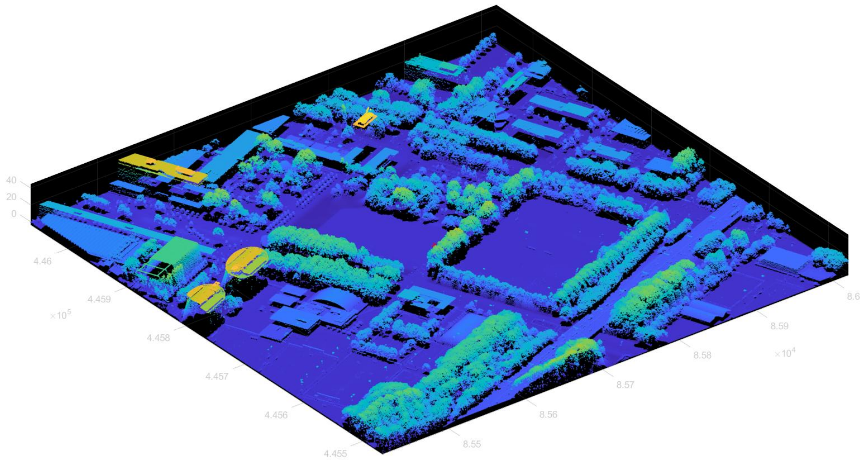

Figure 4.7: Representation of skyline in 3-D

This point cloud is turned into shapes in spherical coordinates through the function ”Horizonscanner”. These shapes are plotted in spherical coordinates of azimuth and altitude.

5

Methodology

A MATLAB model based on Single BRDF is developed. The intensity of reflected light is determined from the Single BRDF. This intensity or irradiance is used to determine the potential of the after-image created by the light. The hazard plot shown in Figure 2.3 is used for this purpose. These reflected light with irradiance, which has a higher potential for after-image creation are mapped on the spherical representation of the skyline. The effect of shadowing of incoming light and obstruction of outcoming light is considered for the projection in spherical projection. Finally, this result is converted into the form of a fish-eye view. The flow of the model development is discussed in detail in the sections below.

5.1. BRDF and Glare Prediction

A new function is developed based on the Single BRDF and Glare prediction from the value of reflected light irradiance. In single BRDF, the vectors shown in Figure 3.1 are converted in form of the input angles. These vectors along with other inputs such as reflection factor, roughness and isotropy factor, and PV panel specifications are then used to determine the value of reflected light in percentages. The value of the BDRF is set as zero when the solar altitude is zero. These values are for a PV located in The Green Village. The Green Village is a field lab for sustainable development on campus. The system placed in one of the roofs of The Green Village has an azimuth of $247°$ and a tilt of $28°$. The are of this system is 3m x 3m which is closer to reality. The value of BRDF throughout the day (on an hourly basis) for this system on four different days is shown in Figure 5.1.

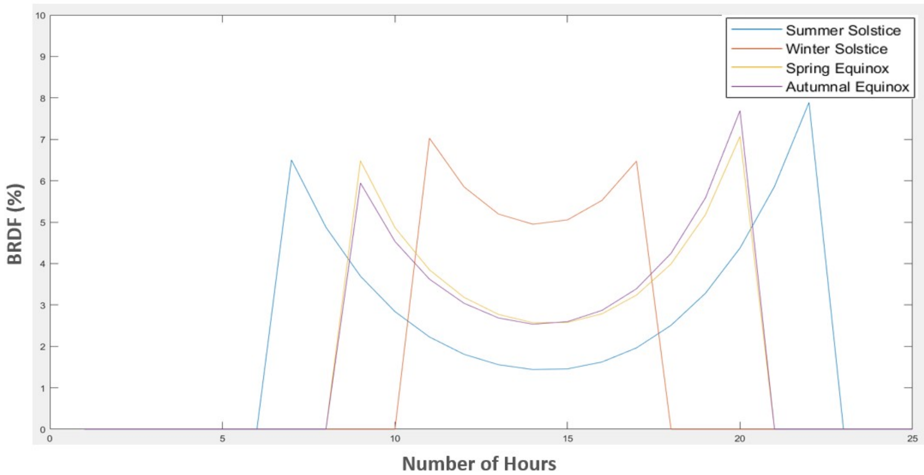

Figure 5.1: PV panel Geometry

There is a low reflection in the afternoon. Meanwhile, the reflection is higher in the morning and evening times. This particular panel is oriented towards the southwest. Hence, the reflection is low in the afternoon as the sun rays face the PV panel[33].

The reflected light percentage is used to determine the irradiance of reflected light. Here, the input irradiance taken to calculate reflected irradiance is DNI as discussed before. This reflected irradiance is assumed as a collimated beam to determine irradiance at the cornea. This is then converted to retinal irradiance as explained before in chapter 3.

This process is repeated for all the available input data. In the case of Meteonorm, this process is repeated every hour. The outputs obtained from this function are the values of reflected light. Whether this light has a high potential to create an after-image, incoming, and outcoming light direction, and the time of the year there is a high potential to create an after-image is given by this function.

5.2. Effect of Urban Construction and Skyline

In an urban environment, buildings and construction can result in shadowing for the PV panels. Additionally, certain buildings also obstruct reflected light. This effect needs to be considered to get results of glare at a certain distance. To achieve this, there needs to be a projection of the skyline or urban construction in form of data; i.e., the creation of shapes in azimuth and the altitude of the construction on the site. This is done through a function called ”Horizonscanner” in MATLAB. The representation of the skyline in spherical coordinates of a site near the Green Village, Delft is shown in Figure 5.2. The radius of the selected site shown in the figure below is 300 m.

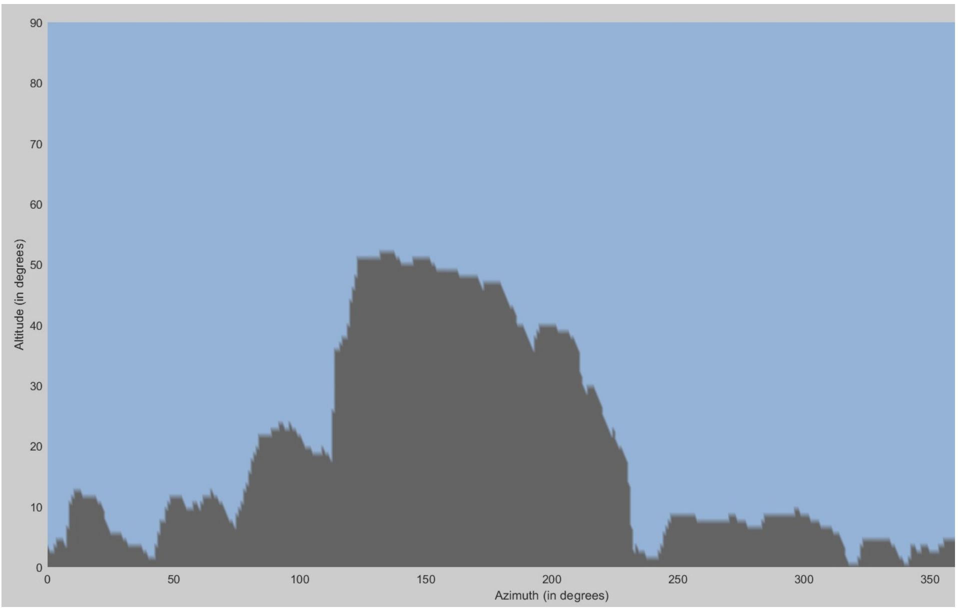

Figure 5.2: Representation of skyline in spherical coordinates

In the figure above, the urban construction is shown in altitude vs azimuth form. Here, the footprint also includes objects such as trees in addition to urban construction.
Using this shape of the skyline, the effect of shadowing and obstruction has to be considered. First, the effect of shadow by a building or construction impeding the incoming sunlight is calculated. This is done by the look-back method. The altitude and azimuth of the incoming light are compared with the shapes formed by the construction. If there is any interference, then the value of BRDF is set as it does not reach the PV panel. The distance up to which this process is done is 1000 m. Similarly, the analysis of obstruction is done. The interference of light to any construction shape before the radius of interest is considered obstruction. In this case, the value of irradiance at the cornea is set as zero.

These results are then projected in spherical coordinates shown in Figure 5.2. The results are also presented in polar coordinates (fish-eye view). The fish-eye view of the location at the Green Village is shown in Figure 5.3.

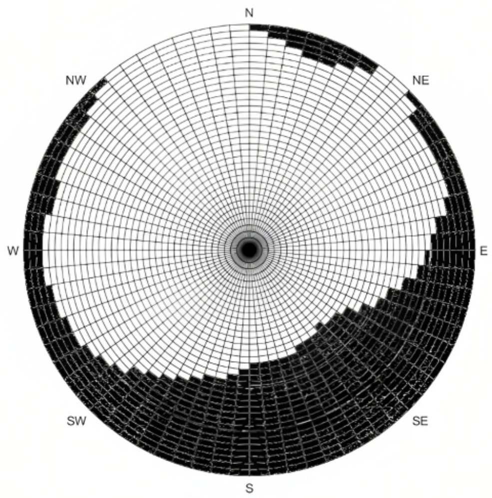

Figure 5.3: Representation of skyline in fish-eye view

The resolution of the result representation in the spherical view and the fish-eye view is different. The resolution in the spherical view depends on the source angle of the system. But the resolution in the fish-eye view depends on the number of slices and rings in the polar plot.

6 Validation

The model newly developed model has to be validated. There are two ways the model is validated. The first is to validate it intensively. To check the reflection experimentally, a site visit has to be performed. The irradiance of the reflected light at a selected site can be found through a light meter or irradiance meter[34]. This value of irradiance can then be used in the Miller-Nadler glare testing machine to determine whether this light can create glare[35]. This result can then be compared with the results obtained from the model. The experimental validation of the model is out of scope and can be performed in the future.

The second way to determine the validity of the model is through a combination of logical arguments and experience. This can then be compared to the results obtained from the model. The first step is to check the value of reflected light in percentage, obtained from the BRDF model to actual reflections reported from PV. The analysis is done for a system located in the Green Village, Delft through this model. The specification of this system has been discussed in chapter 5. The reflection from a PV panel at near normal angles is around 3% which can reach up to about 7.15% as reported by Anurag et al[8]. As shown in Figure 5.1, these values match the reported values of the reflected light.

The light is least reflected the least a few hours after midday. At this time, the Sun's position is southwest as well. Additionally, the value of solar altitude is similar to the panel tilt, hence resulting in low reflection due to light incidence at near normal angle. The value of BRDF (percentage reflected light) is higher during the morning and evening when the angle of incidence is higher. The logic would dictate the BRDF should be lower during the evening than in the morning as the panel is facing southwest. But the value of altitude obtained from Meteonorm (hourly basis) in the evening is lower than in the morning. The first value of altitude in the morning ranges from $3°$-$8°$. Meanwhile, the last value of altitude in the evening ranges from $0.5°$-$5°$. This results in a higher angle of incidence during sunset, which gives a higher value of BRDF. This discrepancy in the altitude is because the data is obtained on an hourly basis.

One of the office locations in the EWI building is selected to validate the reflection direction from the model. This office is located at an angle of $310°$ azimuth from the panel and an angle of $3°$ altitude. This office is located at 310 m distance from the panel site. The office is shown in Figure 6.1. The results of reflection and glare can be shown in Figure 6.2.

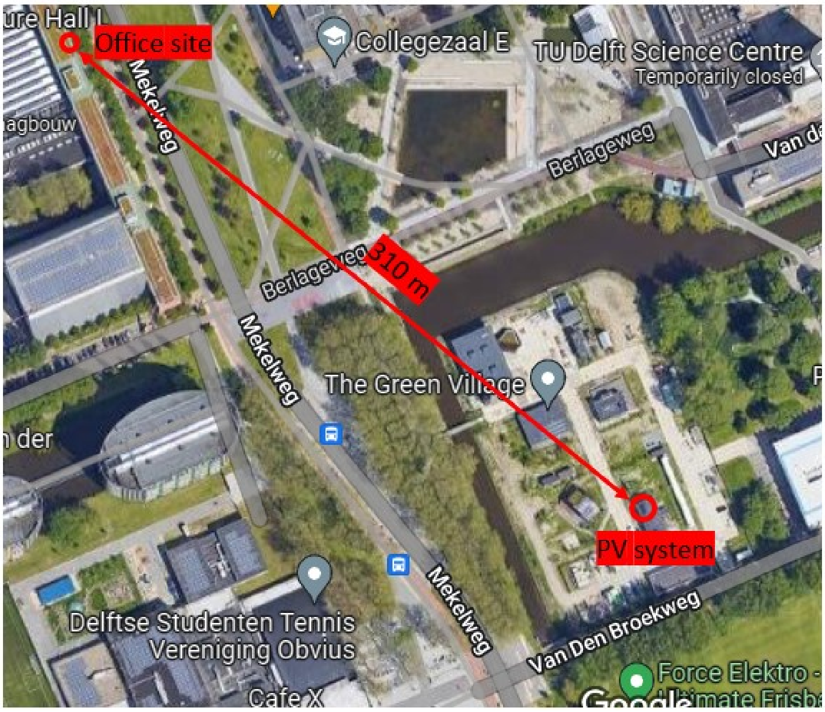

Figure 6.1: Location of office and PV system

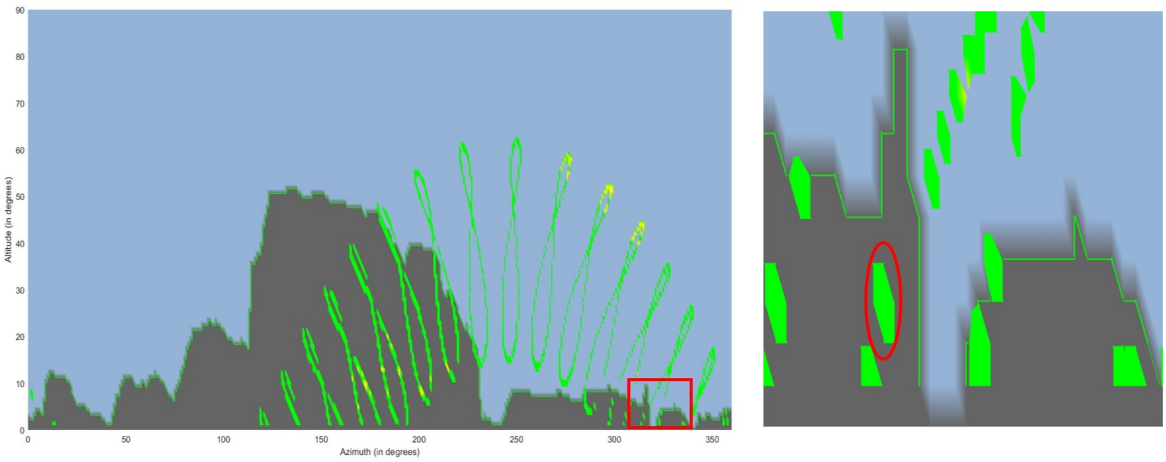

Figure 6.2: Results of reflection and glare from PV system at The Green Village (left), The reflection at selected office site zoomed in (left)

The light is being reflected at the location of the selected office site. The number of reflections at this particular site occurs for 5 hours, a few hours after midday, for a few days in the second week of March. The reflection was also registered at the location in the same time frame. Thus, the directionality of the reflection in the model is validated. There is no validation for the glare conducted for this model due to Miller-Nadler equipment not being available.

7 Results and Discussion

The model developed has been partially validated. The glare created by the PV system in the urban environment can be a source of discomfort. But in areas near airports, railways, and roads, the glare created can result in an accident. Here, the analysis done at one such environment is presented.

As discussed earlier, the installation of PV is becoming more popular at airport sites with the advent of CO2-neutral airports. Hence, there is an urgent need to do glare analysis in these areas. Thus, the analysis was done at the various locations in Schiphol airport in Amsterdam. The results would show the reflection and glare created on the horizon, which would be compared with the hypothetical flight path to check for interference. If a reflection with a low potential for after-image from the PV interferes with the flight path, then the system specification has to be tweaked. If there is glare from the system interfering with the flight path, then the system location has to be reconsidered. Here, four locations selected at the Schiphol airport are discussed. Additionally, the laws and regulations at the airport are discussed as well.

7.1. Laws and Regulations

The laws and regulations involved in the construction and flight paths at airports have to be considered. The airports in India are selected as one of the safest by Airport Council International (ACI)[36]. This is possible due to archaic but safest rules proposed by the Airport Authority of India (AAI). Hence, these laws and regulations are considered because they represent the safest case scenario. The laws and regulations state that a radius of 300m from the ends of the runways is considered a flight path. After that, the funnel shape with extending angle of 35^0 is considered as flight path[37]. Finally, the ascend and the descent of the flight follows the 3:1 rule for stabilized gliding of airplane[38]. This means that the flight travels a distance of 3 nautical miles for an ascend or descent of 1000 feet. This is an international standard.

7.2. Location Selection

There are five runways at Schiphol Airport. These runways are used for flights landing and taking off in different directions. The directions of flight taking off from these runways are shown Table **??** and these runways are shown in Figure 7.1.

Runway	Flight path Landing	Flight path Take-off
Aalsmeerbaan	North	North
Buitenvelderbaan	East	East/West
Kaagbaan	South-east/South-west	South-west
Polderbaan	South	South
Zwanenburgbaan	North/South	North/South

Figure 7.1: Runways at Schiphol Airport[39]

7.3. Application at Selected Location

As Schiphol airport is located in the northern hemisphere, the PV systems are aligned mostly towards the true south. Hence, two locations were selected at Aalsmeerbaan as no flights are approaching and landing from the south direction. Another location is selected at Polderbaan as flights approach from the southwest and there may be interference with reflection and/or glare. The fourth location was selected near Kaagbaan for similar reasons. These locations are mapped as shown in Figures 7.2.

Figure 7.2: First hypothetical PV system near Aalsmeerbaan

7.3.1. Glare Results at Selected Locations

The PV panels hypothesized near the airport locations are assumed to be facing south. Hence, the azimuth of these panels is $180°$. Also, the tilt of the panel is assumed to be $10°$. The tilt of the PV is selected as the least possible value to get the value of reflections throughout the horizon. The size is determined to be 4m x 4m. These values can be changed in the model. The radius of the analysis is determined to be 100 m.

The first location of the system is located about 100 m from the runway Aalsmeerbaan in the east. The system is placed in an open field with a small urban construction as shown in Figure 7.3. The results of reflection and glare are shown in the figures below.

Figure 7.3: First hypothetical PV system near Aalsmeerbaan

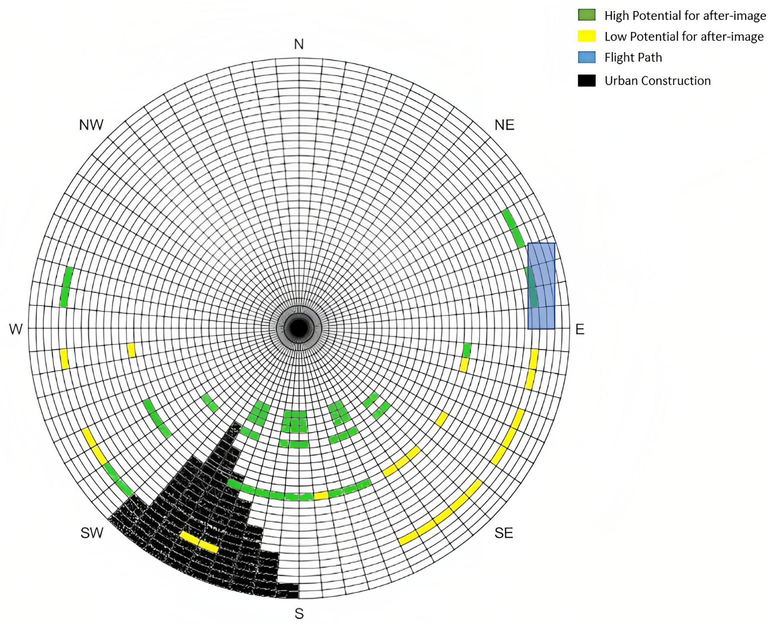

Figure 7.4: Results in the fish-eye view from the first system installed near Aalsmeerbaan

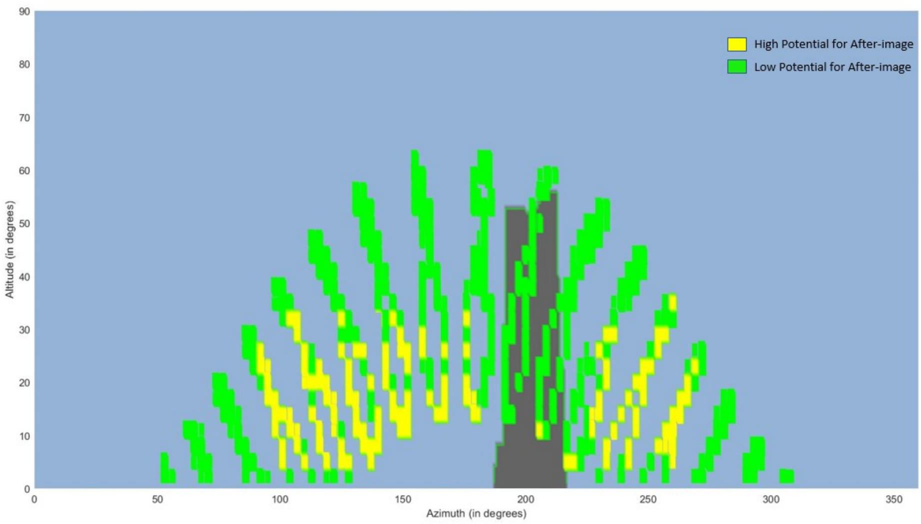

Figure 7.5: Results in the spherical view from the first system installed near Aalsmeerbaan

The first selected location at the west of the runway near Aalsmeerbaan has some interference with the flight path in the east direction as shown in Figure 7.4. The reflection and glare are also shown in Figure 7.5. The reflection from the PV having interference with flight has a low potential for the creation of an after-image. Additionally, the flight here is already on the runway and taxiway bound. Hence, it might not be a huge safety issue.

The second location of the system is located about 1.5 km from the end of the runway of Aalsmeerbaan in the south. The system is placed in an open field without any urban construction or tall vegetation as shown in Figure 7.6. The results of reflection and glare are shown in the figures below.

Figure 7.6: Second hypothetical PV system near Aalsmeerbaan

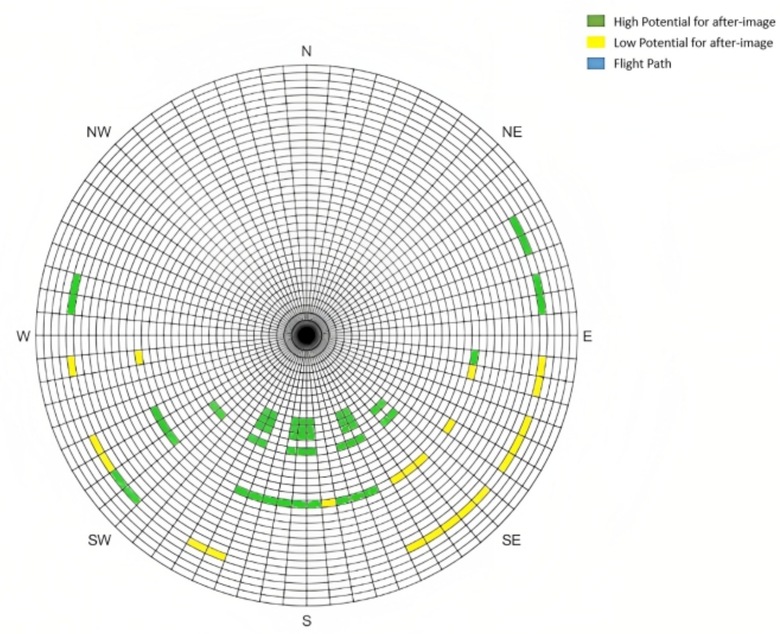

Figure 7.7: Results in the fish-eye view from the second system installed near Aalsmeerbaan

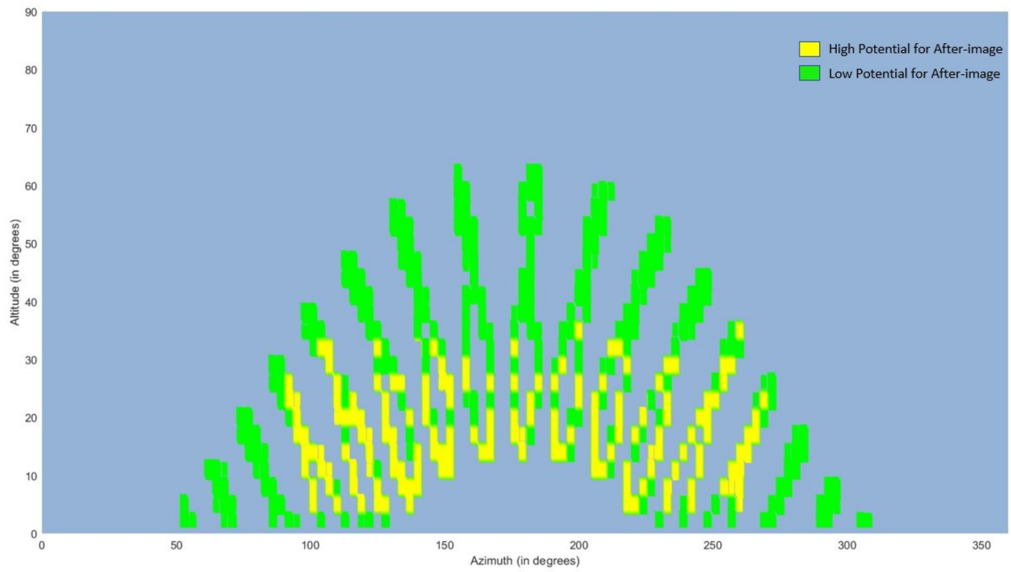

Figure 7.8: Results in the spherical view from the second system installed near Aalsmeerbaan

The results for the second location near Aalsmeerbaan are shown in both spherical and polar projections. The radius of the analysis area is done at 100 m. As this runway is used for only northbound flights and the system is set up south of the runway, there is no interference of the reflection and glare from the PV with the flight path. Hence, this system is viable and can be set up for the future.

Now, the result of the PV located at Kaagbaan is located about 1.8 km southwest of the runway end as shown in the fish-eye view in Figure 7.10. This location is shown in Figure 7.9.

Figure 7.9: Hypothetical PV system near Kaagbaan

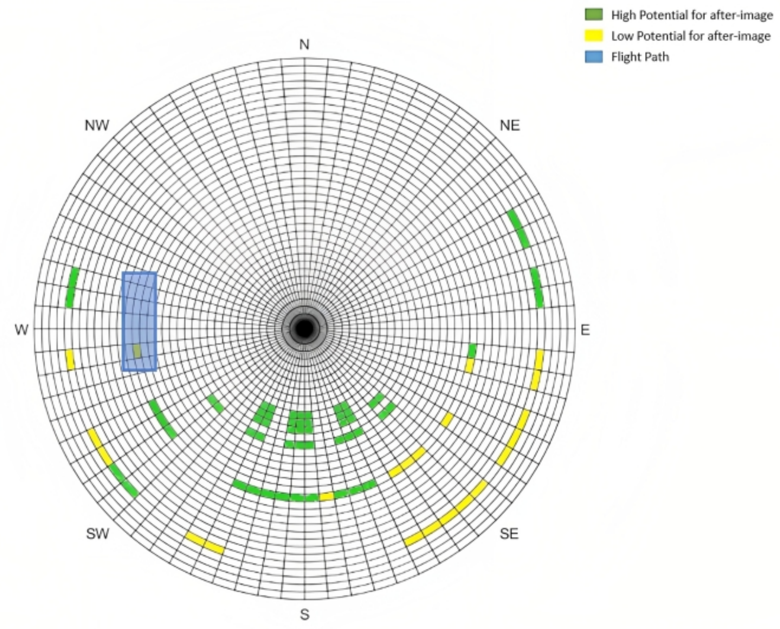

Figure 7.10: Results in the fish-eye view from the third system installed near Kaagbaan

The analysis for this system for glare and reflection is done. The results are shown in a fish-eye view. In Figure 7.10, it is seen that the reflection from the system and the flight path mixes in the east from the PV. The flight path is determined by the 3:1 rule explained before. The issue of glare due to this PV interfering with the flight path occurs every morning between 9 AM-10 AM in the second and third weeks of May. This needs to be considered if the system is installed.

Additionally, the result of glare from PV located at Polderbaan, located about 700 m south of the runway end is shown in the fish-eye view in Figure 7.12.

Figure 7.11: Hypothetical PV system near Polderbaan

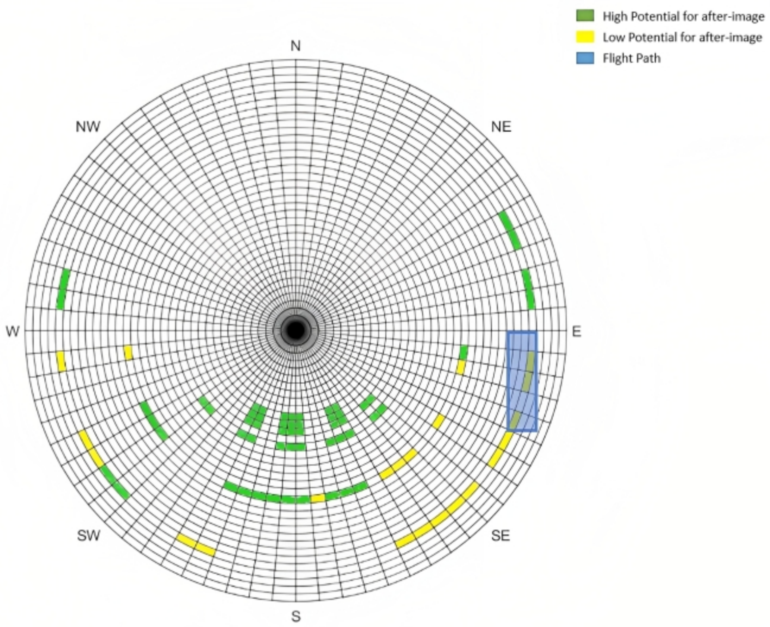

Figure 7.12: Results in the fish-eye view from the fourth system installed near Polderbaan

For this hypothetical system, there are multiple points in the horizon having issues of glare from reflection created by PV which would interfere with the flight path. This glare issue occurs in the third week of February in the late evening, and in the third and fourth weeks of October in the late evening. There are more than 20 occurrences of glare in the flight path in a year due to this PV system. Hence, the location of this PV system needs to be reconsidered, and should not be installed at this location.

Similar analysis can be done for any PV system installed in an urban environment, nearby airports, roads, or railway lines. The path of any locomotive can be projected in the polar plot. Meanwhile, the spherical representation of the reflection shows the number of occurrences in this from the projected path. The time of the year when the glare is created in the horizon at a particular point can be found through MATLAB as well. This model should be used to perform the analysis of the installed PV panels to study the effect of the reflection.

8 Conclusion

The primary objective of this project was to develop a tool to predict the glare occurring from the reflection from the PV system. A tool is developed in MATLAB to accomplish this. The direction and intensity of the reflection are based on a theory of BRDF developed by Schlick. This is used to translate the value to retinal irradiance. Hazard plot developed by Clifford K. Ho is used to determine the potential for the creation of an after-image from the retinal irradiance. The effect of shadowing and obstruction of light due to construction is considered. This model is partially validated through experience with the system at The Green Village. The model is not validated for glare as it requires Miller-Nadler equipment, which can be performed in the future.

The model is applied at four different locations near and around Schiphol airport for 100 m radius. The results of reflection and glare are shown in polar and spherical coordinates. The second system near the Aalsmeerbaan runway can be deemed safe as neither reflection nor glare interferes with the flight path. This system can be installed to get renewable energy for airport use. The first system near the Aalsmeerbaan runway reflects light with low potential for the creation of after-image, hence this system should be reconsidered. The two systems near Polderbaan and Kaagbaan have glare from PV interfering with the flight path. This can be very dangerous and can result in accidents during flight approach or take off. These systems should not be installed in any case. The analysis should also be conducted for the ATC tower in addition to the flight path.

This model can be used for PV systems installed at any location in urban environments, airports, railway lines, and roads. It should be imperative that the model should be used to analyze the glare from the PV system in these environments as the glare can lead to accidents. Finally, in the case of higher levels of glare from PV, the system specifications have to be tweaked or the system needs to be reconsidered to make the urban environments optically safe and comfortable.

References

[1] *The World Bank: Urban Development*. 2022. URL: https://www.worldbank.org/en/topic/urbandevelopment/overview (visited on 11/16/2022).

[2] IEA. “Approximately 100 million households rely on rooftop solar PV by 2030”. In: *IEA, Paris* (2022).

[3] *European airports commit to net zero carbon emissions under their control by 2050*. 2022. URL: https://aci-europe.org/netzero.html (visited on 11/16/2022).

[4] Thomas Rose and Alexander Wollert. “The dark side of photovoltaic — 3D simulation of glare assessing risk and discomfort”. In: *Environmental Impact Assessment Review* 52 (2015), pp. 24–30. ISSN: 0195-9255. DOI: https://doi.org/10.1016/j.eiar.2014.08.005.

[5] Van Nakagawara, Ronald Montgomery, and Kathryn Wood. “Aircraft accidents and incidents associated with visual effects from bright light exposures during low-light flight operations”. In: *Optometry (St. Louis, Mo.)* 78 (Sept. 2007), pp. 415–20. DOI: 10.1016/j.optm.2006.11.016.

[6] Alice Kandt and Rachel Romero. *Siting Solar Photovoltaics at Airport*. 2014.

[7] Kelly Pickerel. *7 cool solar installations at U.S. airports*. 2016. URL: https://www.solarpowerworldonline.com/2016/03/7-cool-solar-installations-at-u-s-airports/ (visited on 08/12/2022).

[8] Anurag Anurag et al. “General Design Procedures for Airport-Based Solar Photovoltaic Systems”. In: *Energies* 10 (Aug. 2017), p. 1194. DOI: 10.3390/en10081194.

[9] S. Sreenath, K. Sudhakar, and A.F. Yusop. “Solar PV in the airport environment: A review of glare assessment approaches metrics”. In: *Solar Energy* 216 (2021), pp. 439–451. ISSN: 0038-092X. DOI: https://doi.org/10.1016/j.solener.2021.01.023.

[10] Clofford K. Ho. “Observations and Assessments of Glare from Heliostats and Trough Collectors: Helicopter Flyover and Drive-By Sightings”. In: *SolarPACES* (2011).

[11] Kevin Wymelenberg and Mehlika Inanici. “A Study of Luminance Distribution Patterns and Occupant Preference in Daylit Offices”. In: (June 2009).

[12] Jan Wienold and Jens Christoffersen. “Towards a new daylight glare rating”. In: *Ludwig Erhard Haus Industrie- und Handelskammer zu Berlin* (Jan. 2005), pp. 157–161.

[13] Greg W. Larson and Rob A. Shakespeare. *Rendering with Radiance. The Art and Science of Lighting Visualization*. 1998.

[14] Giuseppe Iuliano and Laura Bellia. “Daylight Glare: A Review of Discomfort Indexes”. In: (2007).

[15] Antonis Ioannides. “Holladay 2 Formula”. In: *Ophthalmology* 118.12 (2011), p. 2525. ISSN: 0161-6420. DOI: https://doi.org/10.1016/j.ophtha.2011.07.023.

[16] Clifford K. Ho, Cheryl M. Ghanbari, and Richard B. Diver. “Methodology to Assess Potential Glint and Glare Hazards From Concentrating Solar Power Plants: Analytical Models and Experimental Validation”. In: *ASME. J. Sol. Energy Eng.* 133.3 (2011). DOI: https://doi.org/10.1115/1.4004349.

[17] Christophe Schlick. “A Customizable Reectance Model for Everyday Rendering”. In: *Blackwell Science Ltd* 13.3 (1998), pp. 233–246.

[18] Clifford K. Ho and Cianan A. Sims. *Solar Glare Hazard Analysis Tool(SGHAT)*. Sandia National Laboratories. URL: https://www.osti.gov/servlets/purl/1250742 (visited on 03/04/2022).

[19] Mikhail Langovoy and Gerd Wubbeler. *Empirical BRDF models for standard reference materials*. Tech. rep. Physikalisch-Technische Bundesanstalt, Nov. 2013.

[20] Gregory J. Ward. “Measuring and modeling anisotropic reflection”. In: *Proceedings of the 19th annual conference on Computer graphics and interactive techniques* (1992).

[21] Walker HK, Hall WD, and Hurst JW. *Clinical Methods. The History, Physical, and Laboratory Examinations*. 1990.

[22] Gillian Pocock et al. *Human Physiology*. 2013.

[23] Micheal Sutton. *Glint and Glare study*. Tech. rep. Solar Century, May 2020.

[24] Andrew A. Lacis and James Hansen. "A Parametrization for the absorption of solar radiation in the Earth's Atmosphere". In: *The Atmospheric Sciences* 31 (1974), pp. 118–133. DOI: `https://doi.org/10.1175/1520-0469(1974)031<0118:APFTAO>2.0.CO;2`.

[25] *The Definitive Guide to Solar Site Survey*. Solar Power Secrets. URL: `https://solarpanelsvenue.com/solar-mistakes-about-solar-site-survey/`.

[26] *Solar Hybrid Systems. Design and Application*.

[27] Mohamed Khalifa Boutahir et al. "Effect of Feature Selection on the Prediction of Direct Normal Irradiance". In: *Big Data Mining and Analytics* 5 (Dec. 2022), pp. 309 –317. DOI: `10.26599/BDMA.2022.9020003`.

[28] U. Herrmann et al. "5 - System performance measurements". In: *The Performance of Concentrated Solar Power (CSP) Systems*. Ed. by Peter Heller. Woodhead Publishing, 2017, pp. 115–165. ISBN: 978-0-08-100447-0. DOI: `https://doi.org/10.1016/B978-0-08-100447-0.00005-5`. URL: `https://www.sciencedirect.com/science/article/pii/B9780081004470000055`.

[29] Ta-Ko Chuang, A. Usenko, and Jeff Cites. "Bonding Energy of Silicon-to-Glass Wafer Bonding". In: Jan. 2010.

[30] Sadegh Nadimi et al. "Numerical modelling of rough particle contacts subject to normal and tangential loading". In: *Granular Matter* 21 (Oct. 2019), p. 108. DOI: `10.1007/s10035-019-0970-y`.

[31] Romain Guy and Mathias Agopian. *Physically Based Rendering in Filament*. URL: `https://google.github.io/filament/Filament.html`.

[32] J.C. Fernandez-Diaz. "Lifting the Canopy Veil - Airborne LiDAR for Archeology of Forested Areas". In: *Imaging Notes* 26 (2 2011).

[33] *Energy Education*. University of Calgary. URL: `https://energyeducation.ca/encyclopedia/Solar_panel_orientation`.

[34] Peter R. Michael, Danvers E. Johnston, and Wilfrido Moreno. "A conversion guide: solar irradiance and lux illuminance". In: *Journal of Measurements in Engineering* 8 (4 Oct. 2020), pp. 153–166. DOI: `doi.org/10.21595/jme.2020.21667`.

[35] "Chapter 8 - Preliminary examination". In: *The Ophthalmic Assistant (Ninth Edition)*. Ed. by Harold A Stein, Raymond M Stein, and Melvin I Freeman. Ninth Edition. London: W.B. Saunders, 2013, pp. 111–142. ISBN: 978-1-4557-1069-0. DOI: `https://doi.org/10.1016/B978-1-4557-1069-0.00008-6`. URL: `https://www.sciencedirect.com/science/article/pii/B9781455710690000086`.

[36] *Delhi Airport awarded as Best Airport in ACI-ASQ for 2021*. Ministry of Civil Aviation. 2021. URL: `https://www.newdelhiairport.in/blog/best-airport-in-aci`.

[37] Airports Authority of India.

[38] Federal Aviation Administration.

[39] *Flight paths and runway use: How we deploy our runways*. Schiphol. 2022. URL: `https://www.schiphol.nl/en/schiphol-as-a-neighbour/page/flight-paths-and-runway-use/`.

A

Geometry involved in calculating vectors involved in BRDF

Calculating V' vector
$V'_x = sin(\gamma) * sin(\theta')$
$V'_y = cos(\gamma) * sin(\theta')$
$V'_z = cos(\theta')$

Calculating H vector
$H_z = cos(\alpha)$
$H_x = sin(\phi) * sin(\alpha)$
$H_y = cos(\phi) * sin(\alpha)$
$Hd = \sqrt{(}H_z^2 + H_x^2 + H_y^2)$

Getting V vector after tranforming H to [0,0,1]
$V_x1 = real(2 * H_x - V'_x)$
$V_y1 = real(2 * H_y - V'_y)$
$vv = cos(\beta) * Hd$
$uu = (H_x * V_x1) + (H_y * V_y1)$
$ww = uu^2 + (vv^2 * (V_x1^2 * V_y1^2)$
$zz1 = (-uu * H_z + sqrt((uu^2 * H_z^2) - ww * (H_z^2 - vv^2)))/(H_z^2 - vv^2)$
$zz2 = (-uu * H_z - sqrt((uu^2 * H_z^2) - ww * (H_z^2 - vv^2)))/(H_z^2 - vv^2)$
$V_z1 = max([zz1, zz2])$
$Vd = sqrt((V_x1^2) + (V_y1^2) + (V_z1^2))$
$V_x = V_x1/Vd$
$V_y = V_y1/Vd$
$V_z = V_z1/Vd$
$V = [V_x, V_y, V_z]$